ARTICLE

Corrosion behavior of carbon steel coated with a zinc-rich paint containing metallic compounds under wet and dry cyclic conditions

Masamitsu Takahashi[1,2] | **Hiroshi Deguchi[3]** | **Yasunori Hayashi[4]** |
Akihiko Kimura[4] | **Koushu Hanaki[1,5]** | **Hiroaki Tsuchiya[1]** (iD) |
Masato Yamashita[1,5] (iD) | **Shinji Fujimoto[1]** (iD)

[1]Division of Materials and Manufacturing Science, Graduate School of Engineering, Osaka University, Osaka, Japan

[2]Coating Materials Division, NAGASE & CO., LTD., Hyogo, Japan

[3]R&D Center, The Kansai Electric Power Co., Inc., Hyogo, Japan

[4]Institute of Advanced Energy, Kyoto University, Kyoto, Japan

[5]Environmental Material Laboratory, Kyoto Materials Co., Ltd., Kyoto, Japan

Correspondence

Masato Yamashita, Division of Materials and Manufacturing Science, Graduate School of Engineering, Osaka University, 2-1 Yamada-oka, Suita, Osaka 565-0871, Japan and Environmental Material Laboratory, Kyoto Materials Co., Ltd., 2102 Kyodai-Katsura Venture Plaza, 1-39 Goryo Ohara, Nishikyo-ku, Kyoto 615-8245, Japan.
Email: m.yamashita@mat.eng.osaka-u.ac.jp and m.yamashita@kyoto-materials.jp

Abstract

The corrosion behavior of carbon steel coated with a zinc-rich paint containing two metallic compounds, $Al_2(SO_4)_3$ and CaO, as anticorrosive additives was examined under wet and dry cyclic corrosion test conditions. The zinc-rich paint coating without the two metallic compounds formed a white corrosion product and red iron rust on the surface after the corrosion test, whereas the coating with the metallic compounds showed reduced surface corrosion products. The corrosion current density of the painted steel substrate decreased drastically due to the incorporation of metallic compounds in the paint. The zinc-rich paint coating modified with the metallic compounds contained dispersed simonkolleite ($Zn_5(OH)_8Cl_2 \cdot H_2O$) phase and possibly very fine $CaSO_4$ particles, which remarkably improved the protectiveness of the zinc-rich paint coating.

KEYWORDS

atmospheric corrosion, calcium sulfate, carbon steel, metallic compound, rust, simonkolleite, wet and dry cyclic corrosion, zinc-rich paint

1 | INTRODUCTION

Steel is often employed as a structural material in infrastructures. However, the steel used in construction corrodes easily through reactions with corrosive agents, such as oxygen and water, under wet and dry cycles in atmospheric environments. Therefore, effective countermeasures are

required to prevent atmospheric corrosion for maintaining the steel infrastructures.

Several approaches have been proposed and applied to prevent the corrosion of steel, including the application of protective coatings, the inclusion of corrosion inhibitors, and galvanic protection. Among them, a paint coating is the most frequently used protective measure

because of its versatile applicability. In particular, zinc-rich paints are widely used to protect steel infrastructures because of their high anticorrosive properties. The main component of a zinc-rich paint is metallic zinc powder, which is considered to have anticorrosive properties owing to its sacrificial effect as well as the protective effect of its corrosion products.

In general, the anticorrosive properties of conventional paint coatings consisting mainly of a resin are attributed to the barrier effect of the continuous resin-rich film, which prevents the penetration of atmospheric corrosives to the underlying steel substrate. On the other hand, the zinc-rich paint coating exhibits a lower barrier effect because of the lower resin fraction in the film. The main role of the resin in the zinc-rich paint coating is to bind the metallic zinc powder particles in the coating, and the coated film inevitably contains many defects owing to the lower fraction of the resin. Consequently, corrosives from the surrounding environment can easily penetrate the zinc-rich paint coating, and then the corrosion of metallic zinc powder particles results in the generation of alternative paths for corrosives.[1] Moreover, further corrosion of the metallic zinc particles leads to a decrease in their sacrificial anticorrosive effect after the initial stage of corrosion.[2] Therefore, to improve the anticorrosive effect of the zinc-rich paint coating, it is indispensable to increase the protective effect of the corrosion products of Zn.

Effects of alloying elements to metallic zinc coating for steel protection have been intensively investigated. For example, the addition of metallic Al to hot-dipped galvanized coating improved the corrosion protection performance of the coating.[3] Volovitch et al.[4] reported that alloying Al to zinc-based metallic coating stabilized the corrosion products of Zn. As for the zinc-rich paint coating, it was also pointed out that metallic Al added to the coating improved the barrier effect accompanied by the formation of Al oxide.[5] These imply that Al^{3+} eluted from the coatings modified the corrosion products of Zn, resulting in the improved protection of the coatings against corrosion. On the other hand, ion species other than Al^{3+} can also modify the corrosion resistance of Zn. Roventi et al.[6] examined passivating products of Zn in a $Ca(OH)_2$ solution and found that Ca^{2+} progressed the growth of $Ca[Zn(OH)_3]_2 \cdot 2H_2O$ (calcium hydroxyzincate) that passivated Zn surface. In addition, it was reported that SO_4^{2-} in marine droplets decreased the corrosion rate of Zn due to the formation of $NaZn_4Cl(OH)_6\text{-}SO_4 \cdot 6H_2O$ (gordaite).[7] For rust grown on steels, it has been reported that the supply of nonferrous metallic ions to the rusts resulted in the modification of their structure, leading to improvements in the protectiveness of the rusts.[8–12] Furthermore, Kim et al.[9] reported that the supply of metallic cations to a steel surface in the early stage of the corrosion process resulted in the accelerated formation of the protective rust layer. These reports imply that the presence of ion species such as Al^{3+}, Ca^{2+}, and SO_4^{2-} in zinc-rich paint coating from the early stage of corrosion can quickly improve the protective performance of the coating. To achieve a favorable situation in a zinc-rich paint coating, water-soluble metallic compounds are focused.

Recently, our group demonstrated that water-soluble metallic compounds added to an epoxy-based paint provided metallic cations in the paint during the corrosion process, improving the corrosion resistance of the paint-coated steel substrate by modifying the rust structure.[13] Based on the aforementioned discussion, water-soluble metallic compounds added to a zinc-rich paint could modify the corrosion products of Zn, and thus improve the resultant protective effect of the zinc-rich paint coating. In the present study, the structure and protectiveness of the corrosion products formed in zinc-rich paint coatings containing metallic compounds on carbon steel were examined.

2 | EXPERIMENTAL PROCEDURE

2.1 | Specimen

Carbon steel (SS400-JIS G3101) plates with the dimensions of $45\,mm \times 150\,mm \times 3.2\,mm$ were used as the substrate. The surface of the steel plates was treated by grit blast. The specimens were prepared by coating the steel substrates with zinc-rich paints containing $Al_2(SO_4)_3$ and CaO as metallic compounds. The coated zinc-rich paints were cured for 1 week at 23°C and 50% relative humidity (RH). The dry film thickness was approximately $40\,\mu m$.

The amounts of the metallic compounds and zinc powder in the coated films are listed in Table 1. A specimen coated with a metallic-compound-free zinc-rich paint is hereafter referred to as the R-specimen, while the specimen coated with a zinc-rich paint containing $Al_2(SO_4)_3$ and CaO is referred to as the S1-, S2-, or S3-specimen, according to the total amount of $Al_2(SO_4)_3$ and CaO, M_t. The M_t of the S2-specimen is almost twice that of the S1-specimen, while that of the S3-specimen is approximately four times larger. Note that all the paint coatings contained a small amount of conventional pigments, and the rest was epoxy resin.

TABLE 1 Amounts of each metallic compound and zinc powder (mass%) in the zinc-rich paint coatings

Specimen	R	S1	S2	S3
Zn	88.6	87.2	85.8	83.3
$Al_2(SO_4)_3$	0.0	0.8	1.5	2.9
CaO	0.0	0.4	0.7	1.4

2.2 | Wet and dry cyclic corrosion test

Each specimen was subjected to a wet and dry cyclic corrosion test (CCT) in the laboratory. The neutral atmospheric corrosion condition was simulated in accordance with the cycle D method of JIS K 5600-7-9: 2006. The CCT consists of three stages: A salt fog stage with 50 g/L aqueous NaCl solution at 30 ± 2°C for 30 min, a subsequent humid stage at 30 ± 2°C and 95 ± 3% RH for 90 min, and a final dry stage under 50 ± 2°C and then 30 ± 2°C for 2 h each. The pH and the deposition density of the salt fog were 6.6 and 0.02 ml/cm^2/h, respectively.

These three stages were repeated for 360 cycles, which lasted for a total test duration of 2160 h. After the CCT, the specimens were rinsed with deionized water. Finally, their external appearance was compared by photographing with a digital camera.

2.3 | Electrochemical measurements

The electrochemical properties of the specimens were evaluated after the CCT of 2160 h. The specimens were cut into 15 mm × 30 mm coupons and all the sides of the coupons were sealed with a thick epoxy resin film, allowing 15 mm × 20 mm of the specimen surfaces to be exposed to an electrolyte. The electrochemical measurements were conducted in a conventional three-electrode configuration cell with an Ag/AgCl/KCl (3.3 mol/L) reference electrode and a platinum counter electrode using a potentiostat (HZ-5000; Hokuto Denko Co., Ltd.) under the open-air condition at 25°C. A 50 g/L NaCl aqueous solution was used as the electrolyte. After measuring the open-circuit potential for 3 h, the potentiodynamic polarization measurement was performed in the range of ±120 mV from the open-circuit potential at a scan rate of 0.5 mV/s. The corrosion potential (E_{corr}) and corrosion current density (I_{corr}) were estimated by extrapolating the Tafel slopes in the polarization curves. Furthermore, the cathodic polarization curve was also recorded down to a potential of −900 mV.

2.4 | Cross-sectional analysis

The cross-sections of the coated films were observed by field-emission scanning electron microscopy (FE-SEM; Zeiss Ultra 55) at an acceleration voltage of 30 kV, and the elemental distribution in the cross-section of the samples was analyzed by energy-dispersive X-ray spectrometry (Genesis APEXs; AEMTEC Co., Ltd). The specimens were carefully cut for cross-sectional analysis using a diamond grinding wheel.
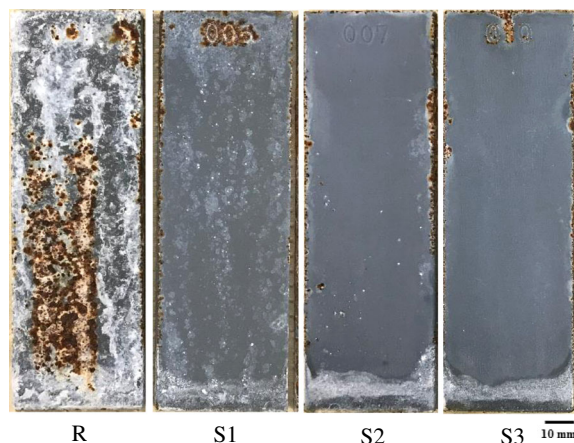

FIGURE 1 Appearance of each specimen surface after 2160 h of the wet and dry cyclic corrosion test [Color figure can be viewed at wileyonlinelibrary.com]

2.5 | X-ray diffraction

The corrosion products formed on the specimens were characterized by X-ray diffraction (XRD). It is very advantageous to employ a highly brilliant X-ray with appropriate energy for the analysis of the corrosion products, which are often composed of fine crystals,[12,14–17] to obtain a highly resolved diffraction spectrum. Therefore, the high-brilliance synchrotron radiation of SPring-8 (Super Photon ring-8 GeV) was used for collecting the XRD data in the present work. The XRD measurements were performed at the BL16XU of SPring-8 for the corrosion products powdered with a pestle and mortar. The X-ray energy was selected to be 15 keV ($\lambda = 0.0827$ nm) to suppress the background signal due to X-ray fluorescence from Zn. X-ray monochromated by passing through a Si(111) double crystal monochromator was irradiated on the powdered corrosion products at an incident angle of 2°. The incident X-ray size was defined at 0.1 mm (height) × 1.0 mm (width) by passing through a four-quadrant slit. Two slits of 0.1 mm (height) × 1.5 mm (width) and 0.2 mm (height) × 2.0 mm (width) were combined to use as the receiving slit.

3 | RESULTS

3.1 | Surface appearance of corroded specimens

Figure 1 shows the appearance of the surfaces of the specimens after 2160 h of the CCT. In the case of the R-specimen, a white corrosion product derived from the metallic zinc powder and red rust from the underlying carbon steel substrate were observed over the entire surface of the coating. On the other hand, the formation
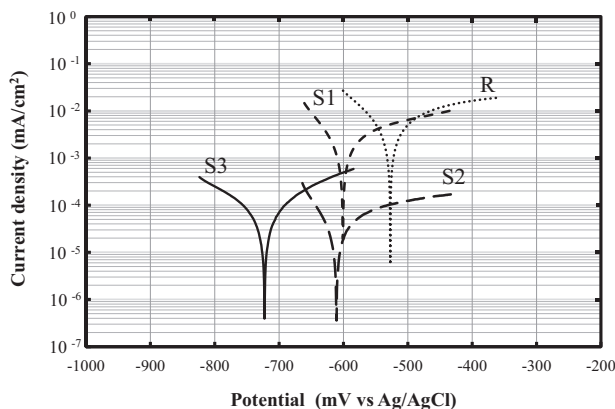
FIGURE 2 Polarization curves obtained from the specimens after 2160 h of the wet and dry cyclic corrosion test

FIGURE 3 Corrosion current density of the specimen as a function of the total amount of the metallic compounds in the zinc-rich paint after 2160 h of the wet and dry cyclic corrosion test

FIGURE 4 Cathodic polarization curves of the specimens coated with zinc-rich paints (with and without the metallic compounds) after 2160 h of the wet and dry cyclic corrosion test

of white corrosion products and red rust was evidently suppressed on the surfaces of the specimens coated with the zinc-rich paint containing the metallic compounds. In particular, neither the white corrosion product nor red rust was observed on the S2- and S3-specimens.

3.2 | Electrochemical behavior

Figure 2 presents the polarization curves of the specimens after the CCT. The R-specimen showed a noble E_{corr} of approximately −530 mV as compared with those of the other specimens. The E_{corr} of the S1- and S2-specimens was found to be approximately −600 mV, while the S3-specimen showed the lowest E_{corr} of approximately −720 mV. These results indicate that the addition of metallic compounds to the zinc-rich paint coating shifts the E_{corr} to the less noble direction.

Further, the corrosion current densities of all the specimens were estimated from the polarization curves. Figure 3 shows the effect of the total amount of the metallic compounds, M_t, on the corrosion current density, I_{corr}. The largest I_{corr} was obtained for the R-specimen, which suggests significant corrosion of the underlying steel substrate to form red rust, indicating that the protective effect of the white corrosion product formed on the specimen surface was probably low. On the other hand, the I_{corr} decreased with increasing M_t, indicating that the metallic compounds added to the zinc-rich paint promote the formation of protective corrosion products on the coated film; they suppress the formation of white corrosion products as well as red rust on the surface of the specimens.

In general, the cathodic reaction is the key factor that determines the corrosion rate of steel; it is therefore advantageous to investigate the cathodic polarization behavior of the 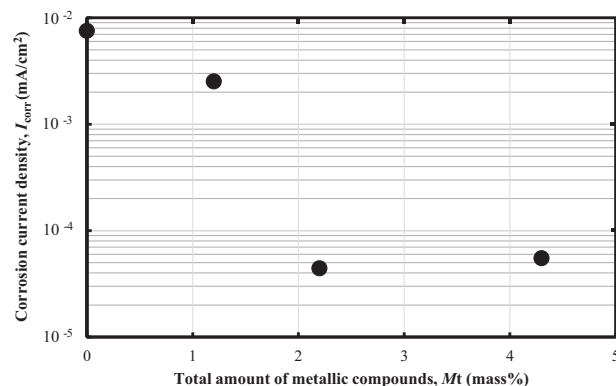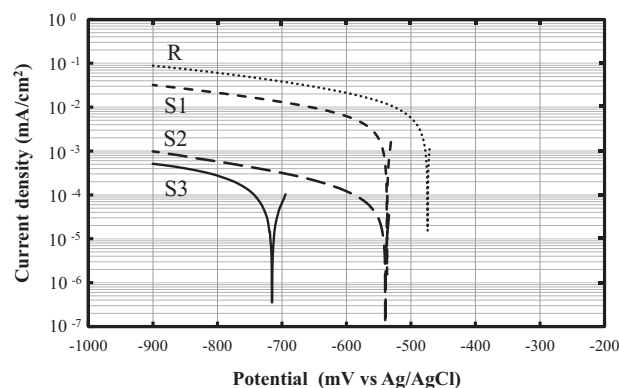specimens. The cathodic polarization curves of the specimens are shown in Figure 4. Extremely low cathodic current densities were confirmed for the S2- and S3-specimens. On the other hand, the cathodic current density of the R-specimen is much larger than the well-known O_2 diffusion-limited current density,[18] which ranges approximately from 10 to 20 $\mu A/cm^2$. This result implies that some reactions other than O_2 reduction could occur on the R-specimen.

3.3 | Elemental distribution along the cross-section

Figure 5 presents the SEM images of the cross-sections and the corresponding elemental distributions for R- and S3-specimens after 2160 h of the CCT. For each sample, the left panel displays the SEM image of the entire film, while the right one shows the magnified image acquired for the portion enclosed by a red rectangle in the image on the left. The brightest part in the Fe mapping image of
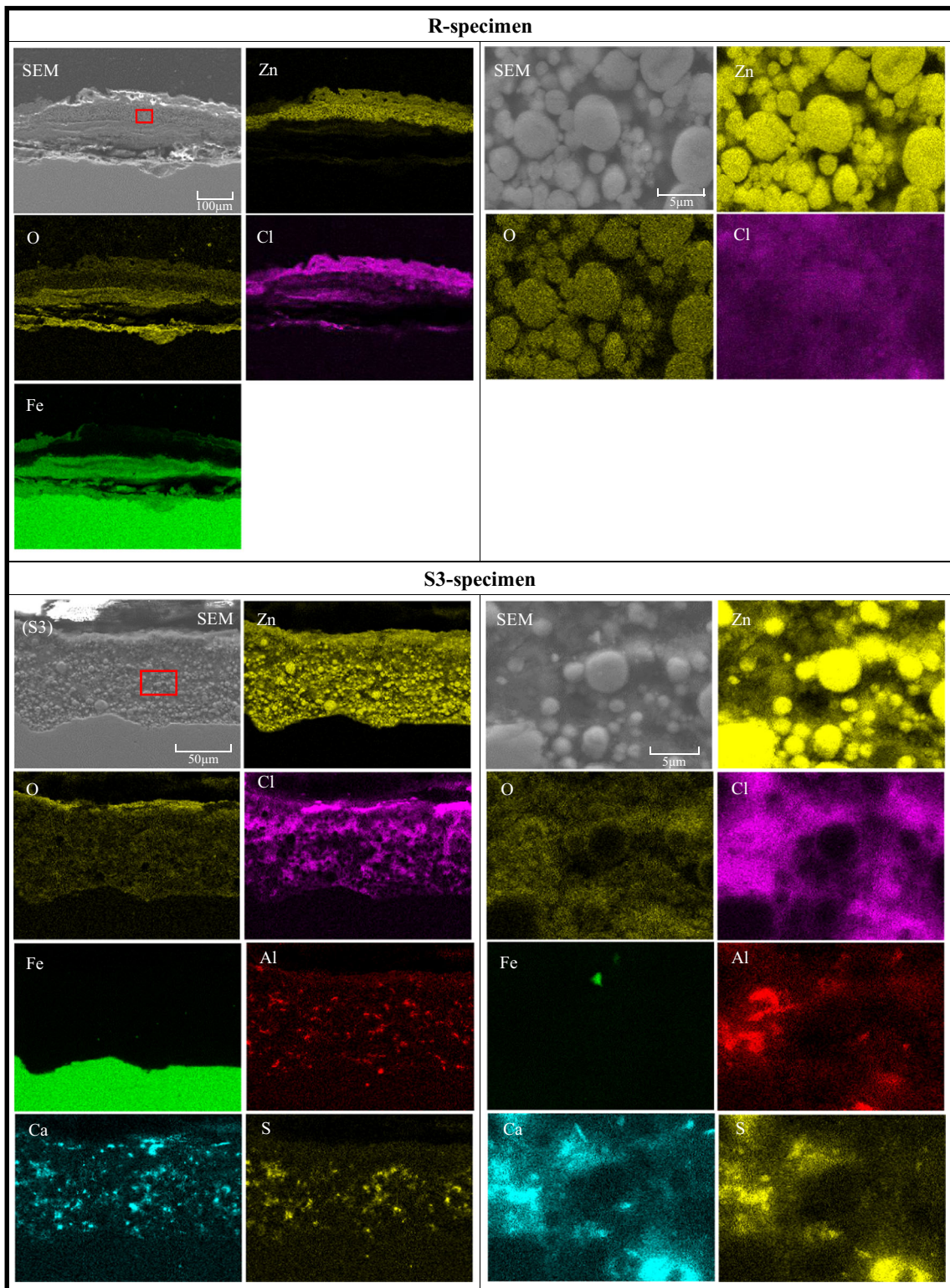
FIGURE 5 Scanning electron microscopy (SEM) images and energy-dispersive X-ray spectroscopic analyses of the cross-sections of the zinc-rich paint coatings for R- and S3-specimens after 2160 h of the wet/dry cyclic corrosion test. The red squares in the SEM images in the left panel indicate the locations from which the higher magnification images in the right panel were captured [Color figure can be viewed at wileyonlinelibrary.com]

the R-specimen on the left panel corresponds to the carbon steel substrate, and the observed Fe distribution over the carbon steel substrate indicates a layered structure of iron rust formed on it. This suggests severe

corrosion of the steel substrate in the case of the R-specimen, indicating that the zinc-rich paint coating without the metallic compounds has poor anticorrosive properties. Zn and Cl were concentrated at the upper part
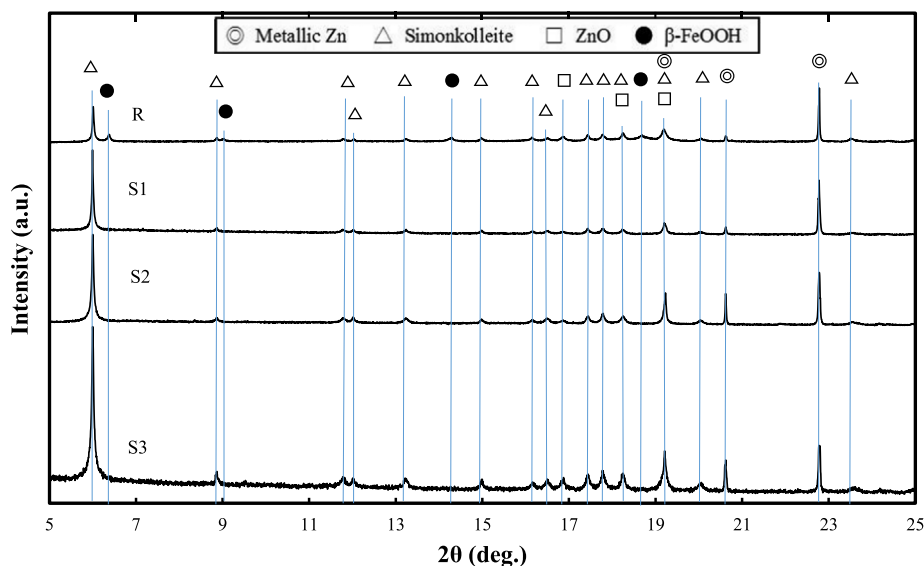
FIGURE 6 X-ray diffraction patterns of the corrosion products of coatings with and without the metallic compounds after 2160 h of the wet and dry cyclic corrosion test [Color figure can be viewed at wileyonlinelibrary.com]

of the coating. In addition, Cl was also enriched at the interface between the paint coating and substrate steel. Furthermore, the magnified mapping images of Zn and O on the right panel indicate that O is mainly located on particulate zinc, which also contains Cl; that is, zinc powder particles were almost oxidized.

For the S3-specimen coated with the zinc-rich paint containing the largest amount of $Al_2(SO_4)_3$ and CaO, on the other hand, Fe was not detected except on the substrate steel, implying that the steel substrate was not corroded during the corrosion test. In addition, the zinc powder particles hardly contained O, as is apparent from the magnified mapping image in the right panel. Moreover, Cl, Al, Ca, and S were also rarely detected at the locations where the zinc powder particles were found. These results indicate that the zinc powder particles mostly remained in the metallic state even after the corrosion test. The magnified elemental mapping image of Zn reveals that Zn was also distributed in other parts of the coating, where zinc powder particles were not present. This Zn distribution approximately overlaps with the distributions of Al, O, and Cl, indicating the formation of certain corrosion products consisting of O, Cl, Zn, and Al in the coating. Furthermore, remarkably, the Ca distribution matched well with the S distribution. As these two elements were not found on the zinc powder particles, it can be inferred that a compound consisting of Ca and S was also formed in the coating during the corrosion test. Similar tendencies were observed for the S1- and S2-specimens, although the data are not presented here.

3.4 | Phase structure of the corrosion product

Figure 6 shows the XRD patterns of the powders of the corrosion products of the specimens after the corrosion test. The XRD peak intensity is normalized to that of the (101) diffraction peak of metallic Zn observed at $2\theta = 22.8°$. As the diffraction peaks derived from metallic Zn were detected in the XRD patterns of all the specimens, it is concluded that some quantity of the metallic zinc powder remained in the paint films after the corrosion test. In addition to the diffraction peaks of metallic Zn, peaks of β-FeOOH (akaganeite) and $Zn_5(OH)_8Cl_2 \cdot H_2O$ (simonkolleite) were mainly detected in the R-specimen, along with the low-intensity peaks of ZnO. For the S1-, S2-, and S3-specimens containing the metallic compounds, most of the diffraction peaks could be assigned to metallic Zn and simonkolleite.

Comparison of the diffraction peak intensity of the simonkolleite phase with that of metallic Zn indicated that the relative diffraction intensity of simonkolleite became stronger with increasing M_t. This indicates an increase in the amount of simonkolleite in the coating owing to the influence of the metallic compounds.

Considering the elemental distribution in Figure 5, the constituents of simonkolleite, Zn and Cl, were uniformly distributed in the coated film of the S3-specimen, whereas these species were localized near the surface of the coating for the R-specimen. That is, simonkolleite was mainly formed inside the coated film of the S3-specimen, while it was formed near the surface of the coated film in the case of the R-specimen.

4 | DISCUSSION

4.1 | Effect of metallic compounds on the structure of corrosion products

As presented in Figure 1, significant amounts of the white corrosion product and red rust were found on the zinc-rich paint coating without the metallic compounds of $Al_2(SO_4)_3$ and CaO, that is, the R-specimen. As shown in Figure 5, Zn, O, and Cl were distributed at similar locations, particularly at the surface of the film, implying that the white corrosion products observed on the R-specimen surface mainly consist of simonkolleite, $Zn_5(OH)_8Cl_2 \cdot H_2O$. This inference is further supported by the XRD analysis in Figure 6. The formation of the simonkolleite phase at the surface of the R-specimen strongly indicates that, in the absence of metallic compounds in the Zn-rich paint, Zn^{2+} cations dissolved from the Zn powder migrate to the external surface of the protective coating, resulting in the formation of white corrosion products, which were found in abundance on this specimen. Furthermore, the Zn powder particles were considered to be almost corroded, forming particulate simonkolleite, because O was particularly concentrated on the Zn powder particles, where Cl was also present, as displayed in the right panel of Figure 5 for the R-specimen. This result indicates that particulate simonkolleite was formed near the original zinc particle site in the coated film. As O was clearly absent around particulate simonkolleite, defects such as crevices and voids were formed between the simonkolleite particles. Therefore, it is deduced that Cl^- ions and water supplied from the corrosion environment easily penetrated the film or passed through the defects in the film, and finally reached the surface of the steel substrate in the case of the R-specimen, leading to the corrosion of the substrate underneath the porous layer consisting of particulate simonkolleite. This is supported by the appearance of the R-specimen in Figure 1, which showed red rust. According to the XRD pattern in Figure 6, the red rust consists of akaganeite (β-FeOOH), the structure of which includes Cl. The akaganeite phase grew at the inner layer of the coating on the R-specimen, where Fe, O, and Cl were concentrated.

The corrosion behavior of the specimen coated with the zinc-rich paint without any additives changed drastically when $Al_2(SO_4)_3$ and CaO were included in the coating. The distribution of O in the coating on the S3-specimen, which was covered with the zinc-rich paint containing the largest amount of metallic compounds, was found to be different from that of the R-specimen. O was not present in the metallic zinc powder particles, as observed in the magnified mapping image in Figure 5,

indicating that the zinc particles mostly remained in the metallic state in the coated film of the S3-specimen. Moreover, it is noteworthy that O, Cl, Zn, and Al were present in the spaces between the metallic zinc powder particles in the film. This indicates that, unlike the case of the R-specimen, the coating with the metallic compounds formed the simonkolleite phase, probably containing Al (hereinafter referred to as Al-containing simonkilleite), around the metallic zinc powder particles. Another interesting feature in the elemental distribution is the similar distribution of Ca and S in the coating of the S3-specimen. This implies the formation of the poorly water-soluble $CaSO_4$ precipitate.

The reasons for the aforementioned changes in the corrosion behavior of the specimen after the addition of metallic compounds into the paint are discussed in the following. The aqueous NaCl solution sprayed during the corrosion test penetrates the coated film through paths, such as interfaces between the metallic zinc powder particles and epoxy resin. Then, pinholes and voids appear owing to the dissolution of the metallic compounds. $Al_2(SO_4)_3$, which is highly soluble in water, dissolves preferentially and undergoes hydrolysis, as shown in the equation given below:

$$Al_2(SO_4)_3 + 2H_2O \rightarrow 2Al(OH)^{2+} + 2H^+ + 3SO_4^{2-}. \tag{1}$$
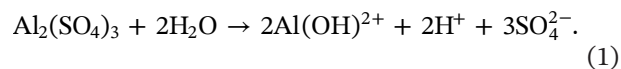
The hydrolysis of $Al_2(SO_4)_3$ lowers the pH of the coating. In fact, a 0.1 M aqueous $Al_2(SO_4)_3$ solution has a pH of 2.9 at room temperature. Roetheli et al.[19] reported that when the pH of the surrounding environment is below 4, the corrosion rate of Zn increases drastically. Thus, if the pH of the coating decreases owing to the hydrolysis of Al^{3+}, the dissolution of the metallic zinc powder is accelerated. The dissolved Zn^{2+} cations could form protective Al-containing simonkolleite in the spaces between the metallic zinc particles, thereby suppressing further dissolution of the metallic zinc particles. In fact, Al-containing simonkolleite remained in the coating on the S3-specimen, whereas the formation of simonkolleite was mainly observed at the surface of the coating film for the R-specimen.

In addition, although CaO included in the paint coating is not necessarily soluble at neutral pH, it dissolves as the pH decreases owing to the hydrolysis of Al^{3+}. The dissolved Ca^{2+} can react with SO_4^{2-} from $Al_2(SO_4)_3$, resulting in the formation of very poorly soluble $CaSO_4$ through a neutralization reaction after the growth of simonkolleite in the coating. The $CaSO_4$ precipitates in the coating after the formation of the simonkolleite phase. As the precipitation occurs within the fine voids in the Al-containing simonkolleite, the

TABLE 2 Structural characteristics of the coated film and corrosion features of R- and S3-specimens after 2160 h of a wet and dry cyclic corrosion test

Specimen	R	S3
Zn particle	Almost oxidized	Almost metal
Simonkolleite location and feature	At the surface of coating film and at Zn particles	Between Zn particles Al incorporated in
Other oxides	Large amount of β-FeOOH	Nano-phase $CaSO_4$
Corrosion rate	High	Very low
Galvanic effect	No	Maintained
Protectiveness of coating film	Poor	Very good

crystal growth of $CaSO_4$ would be restricted remarkably in such fine spaces. No diffraction peaks assignable to $CaSO_4$ were detected in the XRD patterns in Figure 6, supporting the formation of nanophase $CaSO_4$. The occupation of the fine voids in the film by nanophase $CaSO_4$ suppresses further penetration of corrosives, such as Cl^- ions and water. Therefore, the rapid growth of protective simonkolleite and the precipitation of nanophase $CaSO_4$ contribute to the suppressed corrosion of the metallic zinc particles. Thus, a large amount of the metallic zinc powder in the coated films of the S1-, S2-, and S3-specimens remained intact. Nevertheless, a much larger amount of the protective simonkolleite phase is considered to be present in the coating of the S3-specimen with the largest amount of the additives because the relative XRD intensities of the simonkolleite peaks increased with increasing M_t.

4.2 | Effect of metallic compounds on the anticorrosive properties of the zinc-rich paint

We found that not only the corrosion current density, I_{corr}, but also the cathodic current density of the specimens decreased with an increasing amount of the metallic compounds, M_t, in the zinc-rich paint coating. In fact, the I_{corr} and cathodic current density of the S3-specimen were two orders of magnitude lower than those of the R-specimen. These variations are closely related to the structure and properties of the corrosion products.

It is well known that the cathodic reaction on bare steel is O_2 reduction, and the diffusion-limited current density of O_2 reduction ranges approximately from 10 to 20 $\mu A/cm^2$. On the other hand, the cathodic current density at -900 mV for the R-specimen (see Figure 4) was approximately 100 $\mu A/cm^2$. This large cathodic current density can be explained by considering the reduction of β-FeOOH in addition to the reduction of O_2. Moreover, as mentioned above, the coating of the

R-specimen contained defects that allowed Cl^- ions and water to penetrate towards the steel substrate from the external environment. This defective structure of the coating might also lead to the largest I_{corr}. The other feature of the R-specimen is the noble E_{corr} of approximately -530 mV, which falls in the range of the usual corrosion potential of rusted carbon steel,[20] indicating that the galvanic effect of Zn had already disappeared because almost all the metallic zinc powder had corroded to simonkolleite.

Further, for the specimens coated with the zinc-rich paint containing the metallic compounds, a lower I_{corr} was obtained, as shown in Figure 3. In particular, S2- and S3-specimens with an M_t of 2.2 and 4.3, respectively, showed a significantly lower I_{corr} of less than 0.1 $\mu A/cm^2$. This significantly lowered I_{corr} could be attributed to the high protectiveness of the coating. As argued above, in the zinc-rich paint coating with the metallic compounds, the zinc powder particles remained in the metallic state and were surrounded by the protective Al-containing simonkolleite phase as well as very poorly soluble nanophase $CaSO_4$. This hybrid defect-free structure consisting of metallic Zn, Al-containing simonkolleite, and nanophase $CaSO_4$ strongly prevents the penetration of corrosives from the environment. In fact, the enrichment of Cl at the interface between the coating film and steel substrate in the case of the R-specimen was not clearly observed for the S3-specimen, as shown in Figure 5, indicating the high barrier effect of the coating on the S3-specimen even after the corrosion test. In addition, the very low E_{corr} of approximately -720 mV for the S3-specimen is probably due to the sacrificial anode effect of the metallic zinc powder particles remaining in the coating.

In summary, the typical features of the zinc-rich paint coating with the metallic compounds after the corrosion test are listed in Table 2. First, the zinc powder remains in a metallic state. Second, Al-containing simonkolleite forms between the metallic zinc particles, and third, poorly soluble nanophase $CaSO_4$ fills the fine voids between the Al-containing simonkolleite phase. Owing to these novel

features, the zinc-rich paint coating with the metallic compounds shows a long-term galvanic effect.

5 | CONCLUSIONS

The effects of adding metallic compounds, $Al_2(SO_4)_3$ and CaO, to a zinc-rich paint on the protectiveness of the steel substrate were examined through a wet and dry CCT. The following conclusions were drawn:

1. White corrosion products and red rust formed on the surface of the paint film without the metallic compounds. On the other hand, the formation of corrosion products and rusting was significantly suppressed in the case of the zinc-rich paint coating with the metallic compounds.
2. The corrosion potential and corrosion current density decreased drastically with the addition of metallic compounds to the zinc-rich paint.
3. The added metallic compounds maintained the galvanic effect of the zinc powder in the zinc-rich paint coating, leading to improved protectiveness of the coating even after the corrosion test.
4. The improved protectiveness of the coating containing the metallic compounds can be attributed to the formation of dispersed simonkolleite and possibly very fine $CaSO_4$ particles.

ORCID
Hiroaki Tsuchiya https://orcid.org/0000-0001-5619-0139
Masato Yamashita http://orcid.org/0000-0002-8852-6917
Shinji Fujimoto http://orcid.org/0000-0002-7787-4190

REFERENCES
[1] T. Miwa, A. Ishii, M. Watanabe, S. Oka, *Rust Prev. Control* **2019**, *63*, 405.
[2] H. Matsuda, R. Ota, A. Yasuda, A. Yasuda, *Rust Prev. Control* **2017**, *61*, 462.
[3] D. Persson, D. Thierry, N. LeBozec, *Corros. Sci.* **2011**, *53*, 720.
[4] P. Volovitch, T. N. Vu, C. Allély, A. Abdel Aal, K. Ogle, *Corros. Sci.* **2011**, *53*, 2437.
[5] W. B. Chen, P. Chen, H. Y. Chen, J. Wu, W. T. Tsai, *Appl. Surf. Sci.* **2002**, *187*, 154.
[6] G. Roventi, T. Bellezze, E. Barbaresi, R. Fratesi, *Mater. Corros.* **2013**, *64*, 1007.
[7] N. S. Azmat, K. D. Ralston, B. C. Muddle, I. S. Cole, *Corros. Sci.* **2011**, *53*, 1604.
[8] M. Stratmann, K. Bohnenkamp, T. Ramchandran, *Corros. Sci.* **1987**, *27*, 905.
[9] K. Kim, H. Tsuchiya, K. Hanaki, M. Yamashita, S. Fujimoto, *Mater. Trans.* **2020**, *61*, 506.
[10] S. Hayashida, M. Takahashi, H. Deguchi, H. Tsuchiya, K. Hanaki, M. Yamashita, S. Fujimoto, *Mater. Trans.* **2021**, *62*, 781.
[11] M. Yamashita, T. Shimizu, H. Konishi, J. Mizuki, H. Uchida, *Corros. Sci.* **2003**, *45*, 381.
[12] M. Yamashita, H. Miyuki, Y. Matsuda, H. Nagano, T. Misawa, *Corros. Sci.* **1994**, *36*, 283.
[13] M. Takahashi, Y. Hayashi, A. Kimura, K. Hanaki, M. Yamashita, H. Tsuchiya, S. Fujimoto, *J. Soc. Mater. Sci., Jpn.* **2020**, *69*, 797.
[14] M. Yamashita, H. Miyuki, H. Nagano, T. Misawa, *Zairyo-to-Kankyo* **1994**, *43*, 26.
[15] M. Yamashita, T. Misawa, S. J. Oh, R. Balasubramanian, D. C. Cook, *Zairyo-to-Kankyo* **2000**, *49*, 82.
[16] T. Ishikawa, T. Ueno, A. Yasukawa, K. Kandori, T. Nakayama, T. Tsubota, *Corrosion Corros. Sci.*, 2003, *45*, 1037.
[17] R. M. Cornell, U. Schwertmann, *The Iron Oxides*, VCH, Weinheim **1996**.
[18] M. Stratmann, H. Streckel, *Corros. Sci.* **1990**, *30*, 697.
[19] B. Roetheli, G. Cox, W. Littreal, *Met. Alloys* **1932**, *3*, 73.
[20] K. Kim, H. Tsuchiya, K. Hanaki, M. Yamashita, S. Fujimoto, *Corrosion* **2020**, *76*, 335.